

Self-accelerating Topological Photonics

Yiqi Zhang (张贻齐)^{1,2}

¹Key Laboratory for Physical Electronics and Devices,
Ministry of Education, School of Electronic Science and Engineering,
Xi'an Jiaotong University, Xi'an 710049, China

²Shaanxi Key Lab of Information Photonic Technique,
School of Electronic Science and Engineering, Xi'an Jiaotong University, Xi'an 710049, China

(Dated: December 13, 2024)

Both linear and nonlinear self-accelerating valley Hall edge states are predicted in the composited inversion-symmetry-broken photonic graphene lattice with a domain wall. The linear one that is obtained by superimposing a finite-energy Airy envelope to the valley Hall edge state shows self-accelerating, non-diffracting and self-healing properties, with the accelerating trajectory not exactly a parabola. For the nonlinear one which exhibits well self-accelerating and non-diffracting properties that may turn over the moving direction of the valley Hall edge state, it is constructed by superimposing the self-trapped self-accelerating envelope that is obtained from the envelope equation to the valley Hall edge state. The nonlinear self-accelerating valley Hall edge state can circumvent sharp corners without back-scattering, but it is impossible to completely prohibit radiating into the bulk because the topological protection and the self-accelerating demand contrary length of the oscillating tail. The results exhibit the possibility on manipulating topological edge states via self-accelerating waves, and pave the way for the *self-accelerating topological photonics*.

The self-accelerating beam attracts a lot of attentions due to its self-accelerating, non-diffracting, and self-healing properties in last two decades [1–10]. It has been demonstrated that it is impossible to find a rigorous self-accelerating and non-diffracting beam in “static” photonic lattices or straight waveguide arrays [11], but merely self-accelerating Wannier-Stark beams [12, 13]. However, there is also inherent similarity between the Airy beam and the Wannier-Stark beam if the main lobe of the latter is wide sufficiently. Even though the accelerating beams have been reported in photonic lattices [11–18], it is a pity that no work tries to explore the link between the self-accelerating beams [19] and the photonic topological insulators [20–28] to this day. Indeed, this project is still open and elusive since the self-accelerating mechanism may inspire novel ideas on manipulating topological edge states and give birth to a fresh branch of topological photonics.

As to the photonic topological insulator [29, 30] that originates from the solid state physics [31, 32], it has been one of the most interesting research objects in optics/photonics at the moment. The topological edge state which is immune to defects or disorders can propagation unidirectionally without back-scattering or radiating into the bulk [21, 23]. The topologically protected edge state is promising in developing topological lasers [33–37], topological solitons [38–44], and others. It is worth noting that the moving speed of the edge state is fixed that can be predicted from the corresponding band structure directly, which is verified in almost all the present results obtained in both nonlinear and non-Hermitian systems. Finding an effective method to manipulate the moving speed was seemingly uninvolved ever before.

In this Letter, both linear and nonlinear self-accelerating topological edge states are elaborated. The

self-accelerating property can adjust the moving speed and even change the moving direction of the original edge state. Inherited from the self-accelerating beam, the self-accelerating topological edge state can also recover its missing part from it. In nonlinear regime, such self-accelerating can preserve their profile for a long distance without diffraction. By properly apodizing, the self-accelerating topological edge states can be well localized around the valley and can circumvent sharp corner without back-scattering.

The propagation dynamics of the light beam in a photonic lattice can be described by the dimensionless Schrödinger-like paraxial wave equation with cubic self-focusing nonlinearity

$$i\frac{\partial\psi}{\partial z} = -\frac{1}{2}\Delta\psi - \mathcal{R}(x, y)\psi - |\psi|^2\psi, \quad (1)$$

where ψ is the amplitude of the light beam, $\Delta = \partial_x^2 + \partial_y^2$ is the transverse Laplacian, and (x, y, z) are normalized coordinates [45]. The function $\mathcal{R}(x, y) = \sum_{m,n} p_{m,n} \exp(-r_{m,n}^2/d^2)$ describes the lattice waveguide array with the depth $p_{m,n}$, the width d , $r_{m,n}^2 = (x - x_{m,n})^2 + (y - y_{m,n})^2$, and the lattice site coordinate $(x_{m,n}, y_{m,n})$. Typical values for the parameters are: the lattice constant $a = 1.6$, $d = 0.5$, and $p_{m,n} = p \pm \delta$ with $p = 8$ and $\delta = 0.5$. Since the photonic graphene lattice has two sublattices, the inversion symmetry will be broken if one makes the depth of one sublattice be $p - \delta$ and the other sublattice $p + \delta$. In Fig. 1(a), a composited photonic graphene lattice with a domain wall that are composed of two opposite inversion-symmetry-broken photonic graphene lattices is displayed. Note that the domain wall is periodic in y with period $Y = \sqrt{3}a$. It has been demonstrated that the domain wall indicated by the totally blue sites and highlighted

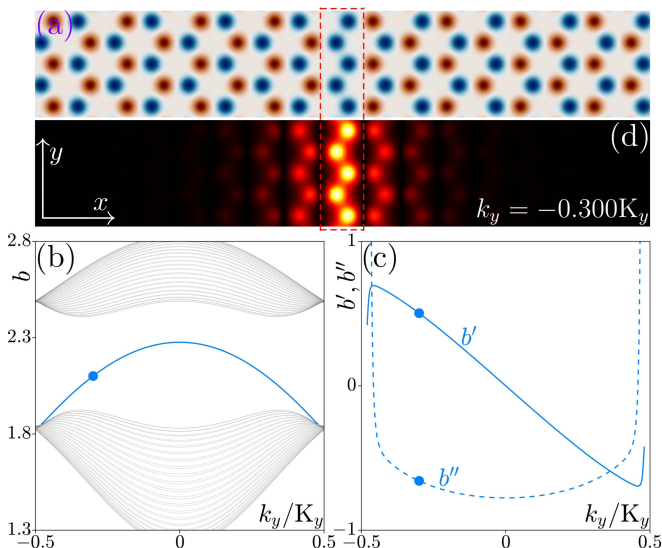


FIG. 1. (a) Inversion-symmetry-broken honeycomb lattice with the domain wall indicated by the dashed rectangle. The depth for the red and blue sites is $p + \delta$ and $p - \delta$, respectively. (b) Band structure of the lattice in (a). The blue and gray lines represent the valley Hall edge state and the bulk states, respectively. (c) First-order (b' , solid line) and second-order (b'' , dashed line) derivatives of the valley Hall edge state in (b). (d) Field modulus profile $|\psi|$ of the valley Hall edge states corresponding to the dot. Panels in (a,d) are shown in $-20 \leq x \leq 20$ and $-3.5 \leq y \leq 3.5$.

with a dashed rectangle supports the topological valley Hall edge state [42, 43, 46, 47], since the difference between the two valley Chern numbers of the same valley across the domain wall is 1 [48–50].

The general solution of Eq. (1) can be written as $\psi = u(x, y) \exp(ik_y y + ibz)$ if the lattice is assumed to be limited in x , and one obtains the eigenvalue problem: $bu = \frac{1}{2}(\partial_x^2 + \partial_y^2 + 2ik_y \partial_y - k_y^2)u + \mathcal{R}u + |u|^2 u$ which can be numerically solved for the relation between b and k_y in the first Brillouin zone $[-K_y/2, K_y/2]$ with $K_y = 2\pi/Y$, if the last nonlinear term is neglected. In Fig. 1(b), the band structure of the composited lattice in Fig. 1(a) is displayed. One finds that the valley Hall edge state that is indicated with blue color emerges from the lower bulk band and widely exists in the band gap. Considering that the first-order derivative $b' = db/dk_y$ and the second-order derivative $b'' = d^2b/dk_y^2$ reflect the moving velocity and the dispersion of the state, in Fig. 1(c), they are exhibited by the solid and dashed curves, respectively. Clearly, the valley Hall edge states move in minus y when $k_y < 0$ and they move in positive y when $k_y > 0$ [51]. The valley Hall edge states at $k_y = -0.3K_y$ is displayed in Fig. 1(d), which is mainly localized on the domain wall with only a fraction of it penetrating into the bulk.

As well known that the valley Hall edge state moves along the domain wall with a fixed velocity $v = -b'$ without radiating into the bulk, and the speed is

nearly unaffected no matter whether it is artificially localized (e.g., by superimposing a Gaussian envelope) in linear regime or it forms an edge soliton in the nonlinear regime. Here, an Airy function with finite integration $\mathcal{A}(y) = \text{Ai}(\alpha y) \exp(\beta \alpha y)$ is superimposed to the valley Hall edge state at $z = 0$ to obtain $\psi(x, y) = \mathcal{A}(y)u(x, y) \exp(ik_y y)$ — the self-accelerating modulated valley Hall edge state [cf. the panel with $z = 0$ in Fig. 2(b)]. The parameters α and β are used to adjust the width of the oscillating humps and ensure containment of the infinite oscillating tail, respectively. For the valley Hall edge state at $k_y = 0$, as indicated in Fig. 1(d), its moving speed is 0 and it should not move during propagation. However, as shown in Fig. 2(a), it bends during propagation after self-accelerating modulation. Note that only the cross-section of the self-accelerated valley Hall edge state in the plane $x = 0$ is tracked with propagation distance z . The dashed curve that is approximately $y = 0.002z^2$, is the fitting trajectory of the self-accelerating valley Hall edge state, which explicitly deviates from the original trajectory indicated by the solid line. It is worth noting that even though the trajectory is a parabola, the coefficient 0.002 is distinct from 0.25 which is the coefficient of the parabolic trajectory of the finite-energy Airy beam in the free space. As illustration, the field modulus profile of the self-accelerating valley Hall edge state at $z = 0$ and 100 are also displayed in Fig. 2(b). Similar to the finite-energy Airy beam in the free space [1, 2], the self-accelerating valley Hall edge state can maintain its profile in a certain distance with the width of the main lobe nearly unchanged (i.e., non-diffracting), but it spreads to lose the property of self-acceleration after a long distance ultimately.

Since the superimposed finite-energy Airy envelope drags the valley Hall edge state to bend in positive y direction, one may imagine that the moving speed of the original valley Hall edge state that moves in negative y direction will be reduced, while the one that moves in positive y direction will be increased. In Fig. 2(c), the propagation of the self-accelerated valley Hall edge state at $k_y = -0.3K_y$ is displayed. Clearly, the trajectory of the modulated beam that is shown by the dashed line, again deviates from its original trajectory indicated by the solid line $y = -b'z$, and the dashed line can be approximately described by $y = -b'z + 0.002z^{1.95}$ with $b' \sim 0.5029$ which is not a parabola any longer. As a counterpart of the valley Hall edge state at $k_y = -0.3K_y$, the valley Hall edge state at $k_y = 0.3K_y$ moves in positive y direction, and the propagation of the corresponding self-accelerating valley Hall edge state is displayed in Fig. 2(d). The trajectory is approximately described by $y = -b'z + 0.002z^{1.82}$ with $b' \sim -0.5029$. One of the promising features of the accelerating Airy beam is its self-healing property [4]. Thus, it is natural to wonder whether this property is preserved here or not. By eliminating the main lobe of the Airy envelope, the prop-

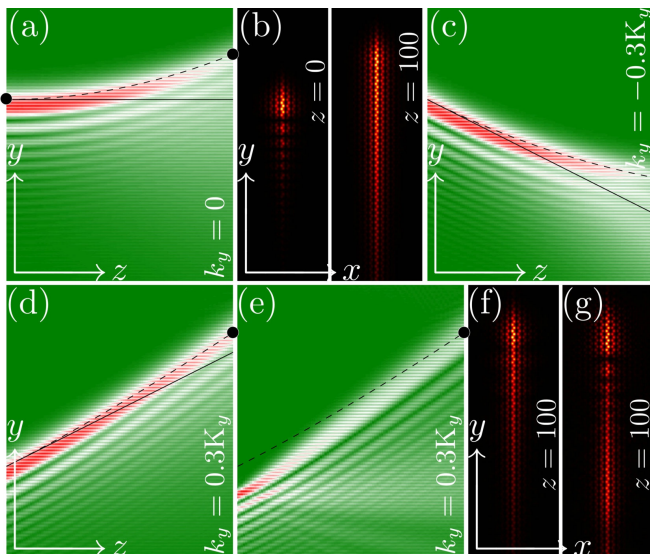


FIG. 2. (a) Cross-section $|\psi(x=0, y)|$ of the valley Hall edge state at $k_y = 0$ [cf. Fig. 1(d)] superimposed with a finite-energy Airy envelope with $\alpha = 0.25$ and $\beta = 0.2$. The dashed line is the fitting trajectory of the self-accelerating valley Hall edge state, and the solid line is that of the valley Hall edge state. Panel is shown in $0 \leq z \leq 100$ and $-60 \leq y \leq 60$. (b) Field modulus profiles of the self-accelerating valley Hall edge state at certain distances that are corresponding to dots in (a). Panels are shown in $-20 \leq x \leq 20$ and $-60 \leq y \leq 60$. (c,d) Setup is as (a,b) but for the edge state at $k_y = -0.3K_y$ [cf. Fig. 1(e)] and $k_y = 0.3K_y$, respectively. (e) Self-healing of the eliminated main lobe of (d). (f,g) Field modulus profiles of the self-accelerating valley Hall edge state at $z = 100$ that are corresponding to the dots in (d,e), respectively.

agation of this self-accelerating valley Hall edge state demonstrates that the main lobe indeed recovers itself and the self-accelerating valley Hall edge state inherits the self-healing property from the Airy beam, as shown in Fig. 2(e). The field modulus profiles of the valley Hall edge state at $z = 100$ in both Figs. 2(d) and 2(e) are displayed in Figs. 2(f) and 2(g), respectively. A comparison between the results also demonstrate that the main lobe of the self-accelerating valley Hall edge state is self-healed. In addition, one finds that the separation between the main lobe and the secondary lobes is more evident in Fig. 2(e) than that in Fig. 2(d).

After discussing the linear self-accelerating valley Hall edge states, the investigation on the nonlinear ones should be launched now and the last term in Eq. (1) cannot be neglected. By plugging the ansatz $\psi = \chi^{-1/2} \mathcal{A}(\eta, z) u(x, y) \exp(ik_y y + ibz)$ into Eq. (1) and following the algebras developed previously [41, 52], one obtains the nonlinear Schrödinger-like equation for the envelope \mathcal{A} : $i\partial_z \mathcal{A} = -\frac{1}{2} \partial_\eta^2 \mathcal{A} - |\mathcal{A}|^2 \mathcal{A}$, in which $\eta = (-b'')^{-1/2}(y + b'z)$ and $\chi = \int_{-\infty}^{+\infty} dx \int_0^y dy |u|^4$. It has been demonstrated that the above equation possesses self-accelerating self-trapped solutions [53–55],

which exhibit parabolic trajectories. Considering the case at $k_y = 0$ in Fig. 2 accelerates in a parabolic trajectory (for the states with $k_y \neq 0$, their trajectories are not but close to a parabola), the nonlinear self-accelerating valley Hall edge state is assumed to accelerate in a parabolic trajectory. To this end, the traveling variable $\eta - \mu z^2$ is substituted for η , one obtains $i\partial_z \mathcal{A} = i2\mu z \partial_\eta \mathcal{A} - \frac{1}{2} \partial_\eta^2 \mathcal{A} - |\mathcal{A}|^2 \mathcal{A}$, where μ is an undetermined coefficient. Assuming its solution can be written with the form $\mathcal{A}(\eta, z) = w(\eta) \exp(i2\mu\eta z + i2\mu^2 z^3/3)$, then one obtains the ordinary differential equation: $\partial_\eta^2 w + 2|w|^2 w - 4\mu\eta w = 0$, with the asymptotic behavior $w(\eta) = \sigma \text{Ai}(\eta)$ and $w'(\eta) = \sigma \text{Ai}'(\eta)$ for large enough $\eta > 0$ [56]. Here σ indicates the strength of the nonlinearity. Note that the nonlinear self-accelerating topological edge state may lose the topological protection, the value of σ should be properly chosen. In Fig. 3(a), two nonlinear self-accelerating solutions with $\mu = 0.002$ are displayed. With increasing the value of σ , the amplitude of the envelope increases too. Similar to the Airy function, the nonlinear accelerating solution also has an infinitely long oscillating tail which is not feasible in physics. Therefore, one has to truncate the tail to make the envelope to be finite-energy. In this way, the self-accelerating property can only remain within a finite propagation distance. But one can preserve sufficient long tail to lengthen the self-accelerating distance.

The nonlinear self-accelerating valley Hall edge state is prepared using the envelope and the linear valley Hall edge state. In Fig. 3(b), the propagation dynamics of the nonlinear self-accelerating valley Hall edge state at $k_y = 0$ is displayed, and one finds that it accelerates during nonlinear propagation. Since the infinitely long tail is truncated [cf. the envelopes in Fig. 3(a)], its non-diffracting property is affected. However, its profile, especially the main lobe, nearly remains unchanged over a distance $z \sim 200$. If the envelope is superimposed to the linear valley Hall edge state at $k_y = -0.3K_y$, the propagation dynamics of the corresponding nonlinear self-accelerating valley Hall edge state is displayed in Fig. 3(c). It firstly moves in minus y but finally turns over its moving direction. This phenomenon is induced by the ballistic property of the self-accelerating beam [3, 57], and was never acquired before for the topological edge state. Besides, both the self-accelerating and non-diffracting properties of the nonlinear self-accelerating valley Hall edge state are illustrated incisively and vividly. For the nonlinear self-accelerating valley Hall edge state at $k_y = 0.3K_y$, its propagation dynamics is given in Fig. 3(d). One finds that it always moves in the positive y direction. Different from the cases in Figs. 3(b) and 3(c), the peak amplitude of the beam in Fig. 3(d) reduces during propagation. The reason is that the oscillating tail is truncated which tends to heal itself. This process surely absorbs some energy from the main lobe and dampens the peak amplitude. Another reason is

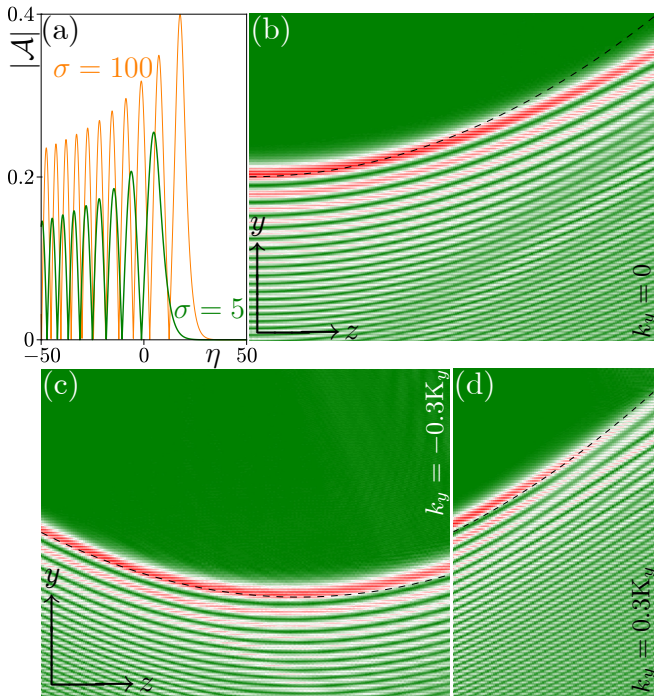


FIG. 3. (a) Self-accelerating solution with $\mu = 0.002$ and different σ . (b) Nonlinear self-accelerating valley Hall edge state with $k_y = 0$, $\chi \approx 0.1592$, $b'' \approx -0.7763$, $\mu = 0.002$, and $\sigma = 5$. (c,d) Same as (b), but for $k_y = -0.3K_y$ and $k_y = 0.3K_y$, respectively. Other parameters: $\chi \approx 0.1663$, $|b'| \approx 0.5029$, and $b'' \approx -0.6584$. (e) Same as (b), but for $\mu = 0.02$. Dashed lines in (b-d) are predicted accelerating trajectories. Panels in (b,c) are shown in $0 \leq z \leq 200$ and $-80 \leq y \leq 80$, while panel in (d) is in $0 \leq z \leq 100$ and $-80 \leq y \leq 80$.

that the truncated beam is not an exact self-accelerating solution any longer. It can only be non-diffracting in a limited distance and then starts to broaden gradually during propagation.

In Figs. 3(b)-3(d), the theoretical trajectories of the nonlinear self-accelerating valley Hall edge states are indicated by dashed lines. Nevertheless, they are not completely in accordance with the real trajectories, and the discrepancy between the theoretical and numerical results is getting bigger with the increasing of the distance. The explanation is that the nonlinear self-accelerating valley Hall edge states in Fig. 3 are truncated (not exact solutions which demand an infinite oscillating tail), which lead to their broadening and damping during propagation. As a result, the trajectories deviate from theoretical predictions. In Fig. 3(c), the theoretical trajectory meets the numerical one quite well [58], because the nonlinear self-accelerating valley Hall edge state moves in the negative y direction which slows down the broadening of the beam and the finite oscillating tail. When the beam starts to move in positive y direction, the trajectories separate from each other. Numerical simulations also demonstrate that if the value of the parameter μ

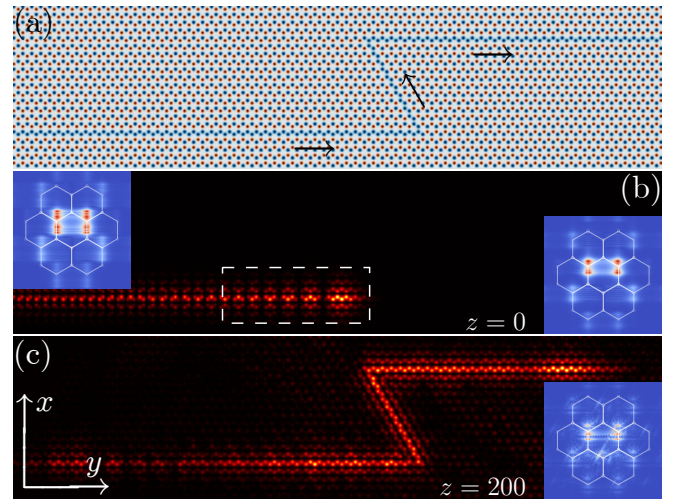


FIG. 4. (a) Composited photonic graphene lattice with a N -path domain wall indicated by the blue color. (b) Nonlinear self-accelerating valley Hall edge state with long tail. The one with short tail is indicated by the part in the dashed rectangle. Left and right insets correspond to the state with long and short tails, respectively. (c) State with short tail at $z = 200$. All panels are shown in $-20 \leq x \leq 20$ and $-100 \leq y \leq 100$. Insets are in $-5 \leq k_{x,y} \leq 5$ with the hexagons being the Brillouin zones.

increases, e.g., from 0.002 to 0.02, the self-accelerating valley Hall edge states behave worse. Conversely, the smaller the value of μ is, the better the behavior of the nonlinear self-accelerating beams will be [12, 13].

For the valley Hall edge state including the valley Hall edge soliton [42, 43], the manifestation of the topological protection is that they can circumvent sharp corner without reflection or radiating into the bulk. Here, a N -shaped domain wall is designed, as shown in Fig. 4(a). Considering that the nonlinear self-accelerating valley Hall edge state at $k_y = 0.3K_y$ always moves in positive y direction [cf. Fig. 3(d)], it is selected as an exemplary object. Investigations demonstrate that the tail affects the self-accelerating edge state in the inverted space greatly. In Fig. 4(b), the self-accelerating edge state has a long tail that reaches $z \sim -200$, and the corresponding scenario in the inverted space shown in the left inset illustrates that most of the energy does not localize to the corners of the Brillouin zone but exhibiting stripe-like distributions that extends to the interior and edges of the Brillouin zone. If the tail of the edge state is short ($z \sim -35$), as shown by the part in the dashed rectangle in Fig. 4(b), localization of the energy will be improved in the inverted space (cf. the right inset). As well known, the corners indicate the locations of the valleys of the band structure [59] and only the light beams in the valleys are well topological protected. Therefore, the requirement to realize the topological protection and that for the self-accelerating property are contradict to each other. Propagation of the nonlinear self-accelerating

valley Hall edge state with short tail shows that the self-accelerating edge state can circumvent sharp corners of the N -shaped domain wall, but meanwhile some energy radiates into the bulk, as shown in Fig. 4(c). Although the topological protection is not ideal, the beam in the inverted space shown in the insets illustrate that there is no back-scattering when it circumvent sharp corners.

Summarizing, both linear and nonlinear self accelerating topological edge states are predicted and analyzed. If the width of the envelop that is superimposed to the topological edge state is broad sufficiently, self-accelerating topological edge states are constructed. The nonlinear self-accelerating topological edge state that may turn over its moving direction during propagation can show non-diffracting property in a quite long distance that is beyond the experimentally observable length. In addition to the topological protection, the self-accelerating topological edge state can also self-heal itself if one part of it is eliminated. These promising results on the self-accelerating topological edge state that indicate the establishment of “*self-accelerating topological photonics*” not only provide an effective tool to manipulate the topological edge state, but also demonstrate the possibility to develop other self-accelerating topological edge states with versatile accelerating trajectories [14, 60] and non-paraxial trajectories [61–67].

This work was supported by the Natural Science Basic Research Program of Shaanxi Province (2024JC-JCQN-06), the National Natural Science Foundation of China (12474337).

-
- [1] G. A. Siviloglou and D. N. Christodoulides, Accelerating finite energy Airy beams, *Opt. Lett.* **32**, 979 (2007).
- [2] G. A. Siviloglou, J. Broky, A. Dogariu, and D. N. Christodoulides, Observation of accelerating Airy beams, *Phys. Rev. Lett.* **99**, 213901 (2007).
- [3] G. A. Siviloglou, J. Broky, A. Dogariu, and D. N. Christodoulides, Ballistic dynamics of Airy beams, *Opt. Lett.* **33**, 207 (2008).
- [4] J. Broky, G. A. Siviloglou, A. Dogariu, and D. N. Christodoulides, Self-healing properties of optical Airy beams, *Opt. Express* **16**, 12880 (2008).
- [5] M. A. Bandres, Accelerating parabolic beams, *Opt. Lett.* **33**, 1678 (2008).
- [6] M. A. Bandres, Accelerating beams, *Opt. Lett.* **34**, 3791 (2009).
- [7] P. Polynkin, M. Kolesik, J. V. Moloney, G. A. Siviloglou, and D. N. Christodoulides, Curved plasma channel generation using ultraintense Airy beams, *Science* **324**, 229 (2009).
- [8] T. Ellenbogen, N. Voloch-Bloch, A. Ganany-Padovicz, and A. Arie, Nonlinear generation and manipulation of Airy beams, *Nat. Photon.* **3**, 395 (2009).
- [9] R. Bekenstein, J. Nemirovsky, I. Kaminer, and M. Segev, Shape-preserving accelerating electromagnetic wave packets in curved space, *Phys. Rev. X* **4**, 011038 (2014).
- [10] M. A. Bandres, I. Kaminer, M. Mills, B. M. Rodriguez-Lara, E. Greenfield, M. Segev, and D. N. Christodoulides, Accelerating optical beams, *Opt. Phot. News* **24**, 30 (2013).
- [11] K. G. Makris, I. Kaminer, R. El-Ganainy, N. K. Efremidis, Z. Chen, M. Segev, and D. N. Christodoulides, Accelerating diffraction-free beams in photonic lattices, *Opt. Lett.* **39**, 2129 (2014).
- [12] R. El-Ganainy, K. G. Makris, M. A. Miri, D. N. Christodoulides, and Z. Chen, Discrete beam acceleration in uniform waveguide arrays, *Phys. Rev. A* **84**, 023842 (2011).
- [13] I. D. Chremmos and N. K. Efremidis, Band-specific phase engineering for curving and focusing light in waveguide arrays, *Phys. Rev. A* **85**, 063830 (2012).
- [14] N. K. Efremidis and I. D. Chremmos, Caustic design in periodic lattices, *Opt. Lett.* **37**, 1277 (2012).
- [15] Y. Kominis, P. Papagiannis, and S. Droulias, Dissipative soliton acceleration in nonlinear optical lattices, *Opt. Express* **20**, 18165 (2012).
- [16] N. M. Lučić, B. M. Bokić, D. Ž. Grujić, D. V. Pantelić, B. M. Jelenković, A. Piper, D. M. Jović, and D. V. Timotijević, Defect-guided Airy beams in optically induced waveguide arrays, *Phys. Rev. A* **88**, 063815 (2013).
- [17] F. Xiao, B. Li, M. Wang, W. Zhu, P. Zhang, S. Liu, M. Premaratne, and J. Zhao, Optical Bloch oscillations of an Airy beam in a photonic lattice with a linear transverse index gradient, *Opt. Express* **22**, 22763 (2014).
- [18] X. Qi, K. G. Makris, R. El-Ganainy, P. Zhang, J. Bai, D. N. Christodoulides, and Z. Chen, Observation of accelerating Wannier-Stark beams in optically induced photonic lattices, *Opt. Lett.* **39**, 1065 (2014).
- [19] N. K. Efremidis, Z. Chen, M. Segev, and D. N. Christodoulides, Airy beams and accelerating waves: an overview of recent advances, *Optica* **6**, 686 (2019).
- [20] L. Lu, J. D. Joannopoulos, and M. Soljačić, Topological photonics, *Nat. Photon.* **8**, 821 (2014).
- [21] T. Ozawa, H. M. Price, A. Amo, N. Goldman, M. Hafezi, L. Lu, M. C. Rechtsman, D. Schuster, J. Simon, O. Zilberberg, and I. Carusotto, Topological photonics, *Rev. Mod. Phys.* **91**, 015006 (2019).
- [22] D. Smirnova, D. Leykam, Y. Chong, and Y. Kivshar, Nonlinear topological photonics, *Appl. Phys. Rev.* **7**, 021306 (2020).
- [23] M. Segev and M. A. Bandres, Topological photonics: Where do we go from here?, *Nanophoton.* **10**, 425 (2021).
- [24] M. Parto, Y. G. N. Liu, B. Bahari, M. Khajavikhan, and D. N. Christodoulides, Non-Hermitian and topological photonics: optics at an exceptional point, *Nanophoton.* **10**, 403 (2021).
- [25] Q. Yan, X. Hu, Y. Fu, C. Lu, C. Fan, Q. Liu, X. Feng, Q. Sun, and Q. Gong, Quantum topological photonics, *Adv. Opt. Mater.* **9**, 2001739 (2021).
- [26] X. Zhang, F. Zangeneh-Nejad, Z.-G. Chen, M.-H. Lu, and J. Christensen, A second wave of topological phenomena in photonics and acoustics, *Nature* **618**, 687 (2023).
- [27] Z.-K. Lin, Q. Wang, Y. Liu, H. Xue, B. Zhang, Y. Chong, and J.-H. Jiang, Topological phenomena at defects in acoustic, photonic and solid-state lattices, *Nat. Rev. Phys.* **5**, 483 (2023).
- [28] W. Yan, B. Zhang, and F. Chen, Photonic topological insulators in femtosecond laser direct-written waveguides, *nphj Nanophoton.* **1**, 40 (2024).

- [29] Z. Wang, Y. Chong, J. D. Joannopoulos, and M. Soljačić, Observation of unidirectional backscattering-immune topological electromagnetic states, *Nature* **461**, 772 (2009).
- [30] M. C. Rechtsman, J. M. Zeuner, Y. Plotnik, Y. Lumer, D. Podolsky, F. Dreisow, S. Nolte, M. Segev, and A. Szameit, Photonic Floquet topological insulators, *Nature* **496**, 196 (2013).
- [31] M. Z. Hasan and C. L. Kane, Colloquium: Topological insulators, *Rev. Mod. Phys.* **82**, 3045 (2010).
- [32] X.-L. Qi and S.-C. Zhang, Topological insulators and superconductors, *Rev. Mod. Phys.* **83**, 1057 (2011).
- [33] G. Harari, M. A. Bandres, Y. Lumer, M. C. Rechtsman, Y. D. Chong, M. Khajavikhan, D. N. Christodoulides, and M. Segev, Topological insulator laser: Theory, *Science* **359**, eaar4003 (2018).
- [34] M. A. Bandres, S. Wittek, G. Harari, M. Parto, J. Ren, M. Segev, D. N. Christodoulides, and M. Khajavikhan, Topological insulator laser: Experiments, *Science* **359**, eaar4005 (2018).
- [35] B. Bahari, A. Ndao, F. Vallini, A. El Amili, Y. Fainman, and B. Kanté, Nonreciprocal lasing in topological cavities of arbitrary geometries, *Science* **358**, 636 (2017).
- [36] Y. Zeng, U. Chattopadhyay, B. Zhu, B. Qiang, J. Li, Y. Jin, L. Li, A. G. Davies, E. H. Linfield, B. Zhang, Y. Chong, and Q. J. Wang, Electrically pumped topological laser with valley edge modes, *Nature* **578**, 246 (2020).
- [37] H. Zhong, Y. D. Li, D. H. Song, Y. V. Kartashov, Y. Q. Zhang, Y. P. Zhang, and Z. Chen, Topological valley Hall edge state lasing, *Laser Photon. Rev.* **14**, 2000001 (2020).
- [38] Y. Lumer, Y. Plotnik, M. C. Rechtsman, and M. Segev, Self-localized states in photonic topological insulators, *Phys. Rev. Lett.* **111**, 243905 (2013).
- [39] S. Mukherjee and M. C. Rechtsman, Observation of Floquet solitons in a topological bandgap, *Science* **368**, 856 (2020).
- [40] M. J. Ablowitz and J. T. Cole, Tight-binding methods for general longitudinally driven photonic lattices: Edge states and solitons, *Phys. Rev. A* **96**, 043868 (2017).
- [41] S. K. Ivanov, Y. V. Kartashov, A. Szameit, L. Torner, and V. V. Konotop, Vector topological edge solitons in Floquet insulators, *ACS Photon.* **7**, 735 (2020).
- [42] Q. Tang, B. Ren, V. O. Kompanets, Y. V. Kartashov, Y. Li, and Y. Zhang, Valley Hall edge solitons in a photonic graphene, *Opt. Express* **29**, 39755 (2021).
- [43] B. Ren, H. Wang, V. O. Kompanets, Y. V. Kartashov, Y. Li, and Y. Zhang, Dark topological valley Hall edge solitons, *Nanophoton.* **10**, 3559 (2021).
- [44] W. Zhang, X. Chen, Y. V. Kartashov, V. V. Konotop, and F. Ye, Coupling of edge states and topological Bragg solitons, *Phys. Rev. Lett.* **123**, 254103 (2019).
- [45] For samples fabricated in the fused silica material by using the femto-second laser direct writing technique [28, 30, 68–72], the transverse coordinates (x, y) are normalized to the characteristic scale $r_0 = 10 \mu\text{m}$, and the propagation distance z is normalized to $kr_0^2 \approx 1.1 \text{mm}$ with the $k = 2n_0\pi/\lambda$, the background refractive index $n_0 = 1.45$ and the wavelength in vacuum $\lambda = 800 \text{nm}$. The potential depth p is related with the refractive index change Δn via $p = k^2 r_0^2 \Delta n / n_0$, and $p = 1$ indicates $\Delta n \sim 1.1 \times 10^{-4}$.
- [46] X. Wu, Y. Meng, J. Tian, Y. Huang, H. Xiang, D. Han, and W. Wen, Direct observation of valley-polarized topological edge states in designer surface plasmon crystals, *Nat. Commun.* **8**, 1304 (2017).
- [47] J. Noh, S. Huang, K. P. Chen, and M. C. Rechtsman, Observation of photonic topological valley Hall edge states, *Phys. Rev. Lett.* **120**, 063902 (2018).
- [48] H. Zhong, S. Xia, Y. Zhang, Y. Li, D. Song, C. Liu, and Z. Chen, Nonlinear topological valley Hall edge states arising from type-II Dirac cones, *Adv. Photon.* **3**, 056001 (2021).
- [49] Q. Tang, Y. Zhang, Y. V. Kartashov, Y. Li, and V. V. Konotop, Vector valley Hall edge solitons in superhoneycomb lattices, *Chaos Solitons Fract.* **161**, 112364 (2022).
- [50] Q. Tang, B. Ren, M. R. Belić, Y. Zhang, and Y. Li, Valley Hall edge solitons in the kagome photonic lattice, *Rom. Rep. Phys.* **74**, 504 (2022).
- [51] If the value of δ is changed from 0.5 to -0.5 , the depth of the sites on the domain wall will be all strengthened. The valley Hall edge state will emerge from the upper bulk band, and the corresponding derivatives will be reversed in comparison with those in Fig. 1(c) [43].
- [52] S. K. Ivanov, Y. V. Kartashov, M. Heinrich, A. Szameit, L. Torner, and V. V. Konotop, Topological dipole Floquet solitons, *Phys. Rev. A* **103**, 053507 (2021).
- [53] I. Kaminer, M. Segev, and D. N. Christodoulides, Self-accelerating self-trapped optical beams, *Phys. Rev. Lett.* **106**, 213903 (2011).
- [54] Y. Zhang, M. Belić, Z. Wu, H. Zheng, K. Lu, Y. Li, and Y. Zhang, Soliton pair generation in the interactions of Airy and nonlinear accelerating beams, *Opt. Lett.* **38**, 4585 (2013).
- [55] Y. Zhang, M. R. Belić, H. Zheng, H. Chen, C. Li, Y. Li, and Y. Zhang, Interactions of Airy beams, nonlinear accelerating beams, and induced solitons in Kerr and saturable nonlinear media, *Opt. Express* **22**, 7160 (2014).
- [56] With these boundary conditions, it can be solved by using the ordinary differential equation solver.
- [57] Y. Q. Zhang, M. R. Belić, J. Sun, H. B. Zheng, Z. K. Wu, H. X. Chen, and Y. P. Zhang, Controllable acceleration and deceleration of Airy beams via initial velocity, *Rom. Rep. Phys.* **67**, 1099 (2015).
- [58] See Supplemental Materials for the animation of the propagation corresponding to the case shown in Fig. 3(c).
- [59] In the first Brillouin zone, the \mathbf{K} valleys are at $(\pm 2\pi/3a, 2\pi/3\sqrt{3}a)$ and $(0, -4\pi/3\sqrt{3}a)$, while the \mathbf{K}' valleys are at $(\pm 2\pi/3a, -2\pi/3\sqrt{3}a)$ and $(0, 4\pi/3\sqrt{3}a)$.
- [60] N. K. Efremidis, Accelerating beam propagation in refractive-index potentials, *Phys. Rev. A* **89**, 023841 (2014).
- [61] I. Kaminer, R. Bekenstein, J. Nemirovsky, and M. Segev, Nondiffracting accelerating wave packets of Maxwell's equations, *Phys. Rev. Lett.* **108**, 163901 (2012).
- [62] P. Aleahmad, M.-A. Miri, M. S. Mills, I. Kaminer, M. Segev, and D. N. Christodoulides, Fully vectorial accelerating diffraction-free Helmholtz beams, *Phys. Rev. Lett.* **109**, 203902 (2012).
- [63] P. Zhang, Y. Hu, T. Li, D. Cannan, X. Yin, R. Morandotti, Z. Chen, and X. Zhang, Nonparaxial Mathieu and Weber accelerating beams, *Phys. Rev. Lett.* **109**, 193901 (2012).
- [64] P. Zhang, Y. Hu, D. Cannan, A. Salandrino, T. Li, R. Morandotti, X. Zhang, and Z. Chen, Generation of linear and nonlinear nonparaxial accelerating beams, *Opt. Lett.* **37**, 2820 (2012).
- [65] F. Courvoisier, A. Mathis, L. Froehly, R. Giust, L. Fur-

- faro, P. A. Lacourt, M. Jacquot, and J. M. Dudley, Sending femtosecond pulses in circles: highly nonparaxial accelerating beams, *Opt. Lett.* **37**, 1736 (2012).
- [66] M. A. Bandres and B. M. Rodríguez-Lara, Nondiffracting accelerating waves: Weber waves and parabolic momentum, *New J. Phys.* **15**, 013054 (2013).
- [67] I. Kaminer, J. Nemirovsky, K. G. Makris, and M. Segev, Self-accelerating beams in photonic crystals, *Opt. Express* **21**, 8886 (2013).
- [68] M. S. Kirsch, Y. Zhang, M. Kremer, L. J. Maczewsky, S. K. Ivanov, Y. V. Kartashov, L. Torner, D. Bauer, A. Szameit, and M. Heinrich, Nonlinear second-order photonic topological insulators, *Nat. Phys.* **17**, 995 (2021).
- [69] Y. V. Kartashov, A. A. Arkhipova, S. A. Zhuravitskii, N. N. Skryabin, I. V. Dyakonov, A. A. Kalinkin, S. P. Kulik, V. O. Kompanets, S. V. Chekalin, L. Torner, and V. N. Zadkov, Observation of edge solitons in topological trimer arrays, *Phys. Rev. Lett.* **128**, 093901 (2022).
- [70] A. A. Arkhipova, Y. Zhang, Y. V. Kartashov, S. A. Zhuravitskii, N. N. Skryabin, I. V. Dyakonov, A. A. Kalinkin, S. P. Kulik, V. O. Kompanets, S. V. Chekalin, and V. N. Zadkov, Observation of π solitons in oscillating waveguide arrays, *Sci. Bull.* **68**, 2017 (2023).
- [71] B. Ren, A. A. Arkhipova, Y. Zhang, Y. V. Kartashov, H. Wang, S. A. Zhuravitskii, N. N. Skryabin, I. V. Dyakonov, A. A. Kalinkin, S. P. Kulik, V. O. Kompanets, S. V. Chekalin, and V. N. Zadkov, Observation of nonlinear disclination states, *Light Sci. Appl.* **12**, 194 (2023).
- [72] H. Zhong, V. O. Kompanets, Y. Zhang, Y. V. Kartashov, M. Cao, Y. Li, S. A. Zhuravitskii, N. N. Skryabin, I. V. Dyakonov, A. A. Kalinkin, S. P. Kulik, S. V. Chekalin, and V. N. Zadkov, Observation of nonlinear fractal higher order topological insulator, *Light Sci. Appl.* **13**, 264 (2024).